Solar Physics (2006) 238: 271–292
DOI: 10.1007/s11207-006-0214-2

TWO REGULARITIES IN THE CORONAL GREEN-LINE BRIGHTNESS – MAGNETIC FIELD COUPLING AND THE HEATING OF THE CORONA

O.G. BADALYAN and V.N. OBRIDKO
Pushkov Institute of Terrestrial Magnetism, Ionosphere and Radio Wave Propagation, 142190 Troitsk, Moscow, Russia
(e-mail: badalyan@izmiran.troitsk.ru)

(Received 27 April 2006; accepted 20 August 2006; Published online 14 October 2006)

Abstract. To study the quantitative relationship between the brightness of the coronal green line 530.5 nm Fe XIV and the strength of the magnetic field in the corona, we have calculated the cross-correlation of the corresponding synoptic maps for the period 1977 – 2001. The maps of distribution of the green-line brightness I were plotted using every-day monitoring data. The maps of the magnetic field strength B and the tangential B_t and radial B_r field components at the distance 1.1 $R_\odot$ were calculated under potential approximation from the Wilcox Solar Observatory (WSO) photospheric data. It is shown that the correlation I with the field and its components calculated separately for the sunspot formation zone $\pm 30^\circ$ and the zone $40-70^\circ$ has a cyclic character, the corresponding correlation coefficients in these zones changing in anti-phase. In the sunspot formation zone, all three coefficients are positive and have the greatest values near the cycle minimum decreasing significantly by the maximum. Above 40°, the coefficients are alternating in sign and reach the greatest positive values at the maximum and the greatest negative values, at the minimum of the cycle. It is inferred that the green-line emission in the zone $\pm 30^\circ$ is mainly controlled by B_t, probably due to the existence of low arch systems. In the high-latitude zone, particularly at the minimum of the cycle, an essential influence is exerted by B_r, which may be a manifestation of the dominant role of large-scale magnetic fields. Near the activity minimum, when the magnetic field organization is relatively simple, the relation between I and B for the two latitudinal zones under consideration can be represented as a power-law function of the type $I \propto B^q$. In the sunspot formation zone, the power index q is positive and varies from 0.75 to 1.00. In the zone $40-70^\circ$, it is negative and varies from -0.6 to -0.8. It is found that there is a short time interval approximately at the middle of the ascending branch of the cycle, when the relationship between I and B vanishes. The results obtained are considered in relation to various mechanisms of the corona heating.

1. Introduction

At present, the governing role of the magnetic field in the appearance and cyclic evolution of solar activity is beyond doubt. In particular, it is the magnetic field that determines the variations of the coronal brightness. However, the mechanism of the corona heating and, therefore, of the relationship between the corona brightness and magnetic field, is unclear (see Aschwanden, 2004; Mandrini, Démoulin, and Klimchuk, 2000). For example, Mandrini, Démoulin, and Klimchuk (2000) suggest in their review 22 possible scaling laws for various heating mechanisms, but the

choice of a particular model still remains impossible. This is obviously due to the fact that there are several heating mechanisms, which play different roles in different regions (active regions, quiet Sun, coronal holes). This role, in turn, may be determined by the contribution of the fields of different scales, their internal structures, combination of low and high loops, and contribution of open magnetic fields. Thus, in order to establish the mechanisms through which the magnetic field controls the physical processes in the corona, we have to estimate quantitatively the relationship between the coronal brightness and the magnetic field.

A promising approach would be to correlate the emission characteristics in the coronal green line 530.3 nm with the magnetic field parameters. The line emission characterizes the level of activity in the solar corona. The brightest regions correspond to the dense loops and loop systems, since the emission intensity in this line is proportional to the squared density. The existence of such regions is associated with the coronal magnetic fields and with the general problem of the corona hating. The regions of decreased green-line brightness are genetically associated with coronal holes (e.g., Fisher and Musman, 1975; Letfus, Kulčár, and Sýkora, 1980; Sýkora, 1992; Guhathakurta, Fisher, and Strong, 1996).

Unfortunately, there are few works establishing a relationship between the green-line brightness and magnetic field and based on sufficiently extensive statistical data (e.g., see Guhatakurta, Fisher, and Altrock, 1993; Wang *et al.*, 1997; Rušin and Rybanský, 2002). Guhatakurta, Fisher, and Altrock (1993) compared the coronal emission and magnetic data for 1984 – 1992. They plotted an interesting space–time distribution of the brightness of the green and red coronal lines. One can see that the distribution of the green-line emission is rather similar to that of the magnetic field. Wang *et al.* (1997) used the SOHO LASCO C1 data for five different days. The structure of the magnetic field lines was calculated under potential approximation from the Wilcox Solar Observatory (WSO) data. It turned out that the structure of the magnetic field and that of the green corona agree fairly well. Wang *et al.* (1997) showed that the density at the base of the magnetic flux tubes is related to the magnetic field intensity as $n_{\rm foot} \propto \langle B_{\rm foot} \rangle^{0.9}$. Rušin and Rybanský (2002) considered the relationship between the coronal green-line brightness and the observed photospheric magnetic field in the high- and low-latitude zones.

In Badalyan and Obridko (2004a,b), we have started investigating the coupling between the brightness I of the coronal green line λ 530.3 nm Fe XIV and the magnetic field strength B at the height of the line formation. This coupling was found out to be rather complicated and to depend on the heliolatitude and phase of the cycle. One could say that the governing role in producing conditions for the green-line emission belongs to the magnetic field. The magnetic field acts to form coronal features differing in their physical conditions, mainly, the plasma density. The increase of density in equatorial loops enhances the green-line emission. In rarefied cold features such as coronal holes, the green-line brightness is weakened. Thus, the magnetic field can both enhance and attenuate the emission of the coronal green line.

The cycle dependence of the correlation between the green-line brightness and magnetic field strength is indicative of different effects of the fields of various scales on the coronal emission lines. Besides, this effect is not the same for different time and spatial scales. The data on the coronal X-ray emission obtained with a high spatial resolution are available for about a full solar activity cycle. These data allow us to compare emission of the corona projected on the disk with the evolving active regions over short time intervals. For analyzing the coupling of the magnetic field and coronal brightness over long time intervals, it is reasonable to use the catalogues of the green-line emission data.

The green-line emission index has an important advantage of being determined almost simultaneously for all heliographic latitudes, which allows the solar activity all over the Sun to be studied using similar data. At present, the series of systematic observations of the coronal green line covers nearly six activity cycles. We are using here the database composed by J. Sýkora (Sýkora, 1971; Storini and Sýkora, 1997; Sýkora and Rybák, 2005) and comprising observations at a number of coronal stations.

In this paper, we continue to study the relationship of the coronal green-line brightness (CGLB) with the coronal magnetic field and its components for the period from 1977 to 2001 (activity cycles 21 – 23). Our analysis allows certain inferences concerning the influence of the magnetic fields of different scales on the brightness of the green-line corona in different phases of the solar activity. This approach brings us right to the solution of a very complicated problem of the coronal heating mechanisms.

2. Databases and Calculation Technique

To study the quantitative relationship between the brightness of the coronal green line 530.5 nm Fe XIV and the strength of the coronal magnetic field and its components, we have calculated the cross-correlation of the corresponding synoptic maps for 1977 – 2001. The CGLB distribution maps were based on the patrol data from a number of the coronal stations reduced to a single photometric system. The process of data homogenization is described in Sýkora (1971). The green-line intensities are given in absolute coronal units (a.c.u., a millionth of the brightness at the disk center in a 0.1 nm band of the adjacent continuum) with a step of $\approx 13^\circ$ in longitude (one day) and 5° in latitude. The gaps in observations (about 15% of the days) are filled by interpolation. All data are reduced to the height of 60 in. above the limb. For detailed description of the database, see Storini and Sýkora (1997) and Sýkora and Rybák (2005). Using the plotted maps, we have made a movie to visualize the space–time distribution of CGLB (Badalyan, Obridko, and Sýkora, 2004, 2005). The movie and some additional materials are available on the Internet site *http://helios.izmiran.rssi.ru/hellab/Badalyan/green/*.

The magnetic field in the corona was calculated under potential approximation using the WSO photospheric data downloaded from the Internet *http://quake.stanford.edu/~wso/wso.html*. The initial data – observations of the longitudinal component of the photospheric magnetic field – were then represented as synoptic maps for each Carrington rotation. The coronal magnetic field was calculated by the well-known method described in Hoeksema and Scherrer (1986) and Hoeksema (1991). We have used here a program that allows all magnetic field components to be calculated from the photosphere up to the source surface (Kharshiladze and Ivanov, 1994). We calculated the tangential B_t and radial B_r components of the magnetic field as well as the total strength B (equal to the square root of the sum of the squares of B_t and B_r). The calculations were performed for the distance of 1.1 $R_\odot$ close to the height of $60''$ (arc sec), to which the CGLB values from the above-mentioned database were reduced. The calculations involved summing over 10 harmonics and introducing a polar correction to take into account the lack of reliability of the field measurements at the poles (Obridko and Shelting, 1999). Both the original and calculated magnetic data are limited to the latitude range of $\pm 70^\circ$.

The observed green-line data and the calculated magnetic field were averaged over six successive Carrington rotations. The averaging over such a long time interval actually excludes from consideration the dynamic events for which the potential approximation is incorrect. The smoothed maps obtained make it possible to trace the large-scale, long-lived coronal features at the height of the green-line emission. The CGLB and magnetic field data organized in such a way have an effective spatial resolution of $10-15^\circ$.

In order to express quantitatively the agreement within each pair of the green-line and magnetic-field maps, we calculated the correlation coefficients between these parameters at the points of the synoptic maps, for which the CGLB data were available (i.e., with a step of 13° in longitude and 5° in latitude). The correlation coefficient was calculated both for the broad and for the narrow 10° latitudinal zones. The behavior of the correlation coefficient was studied in more detail for the low-latitude zone $|\varphi| \leq 30^\circ$ and the zone above $|\varphi| \geq 40^\circ$, which will be arbitrarily called a high-latitude zone (the north and south hemispheres are considered together). The total number of points in each zone is about 400, which yields a mean error of each correlation coefficient equal to 0.02 – 0.03. Even at small correlation coefficients, the error does not exceed 0.05.

A few synoptic maps of the magnetic-field strength and coronal green-line brightness are juxtaposed in Figure 1. The first and the third rows of the maps represent the field strength in the corona, and the second and the fourth rows the distribution of the green-line emission. The maps refer to various phases of cycle 21. The averaging interval is indicated over each pair of maps. The darker areas correspond to greater values of the parameters under discussion; white areas denote small values. The maximum number of tone shades on maps is 8. The solid lines are the isolines of the field strength and green-line brightness (see Table I). The

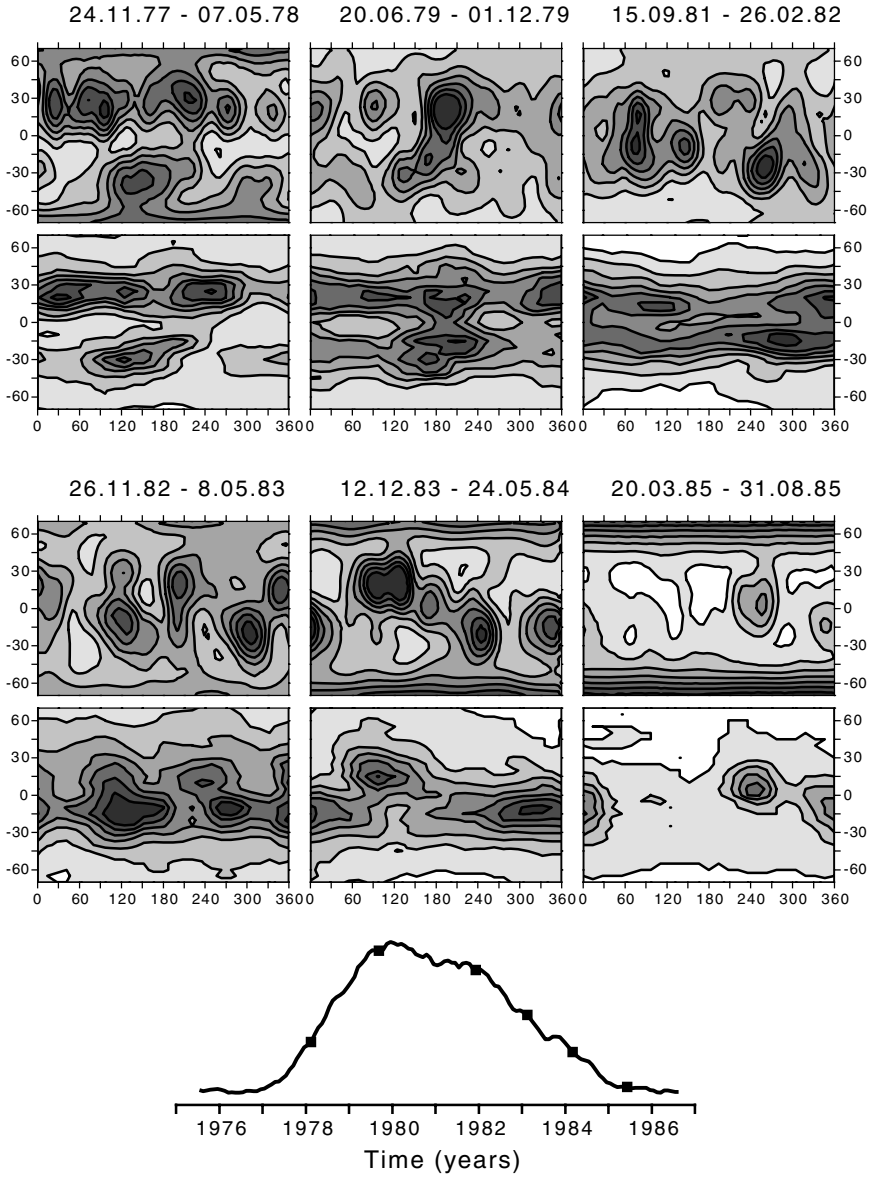

Figure 1. Synoptic maps of the magnetic field strength (*first and third rows*) and coronal green-line brightness (*second and fourth rows*). Positions of the corresponding time interval are indicated on the Wolf number curve for cycle 21 (the *lower plot*). Each map is based on the data averaged over six successive Carrington rotations. *Darker regions* correspond to greater values of the corresponding parameters. *Lines* on maps are the isolines of the magnetic field strength and coronal green-line brightness (see Table I).

TABLE I
Correlation coefficients between the CGLB and the magnetic field strength.

CR	Time interval	B_{max}	ΔB	I_{max}	ΔI	$\|\varphi\| \leq 30^\circ$	$\|\varphi\| \geq 40^\circ$
1662 – 1667	24-11-77 – 07-05-78	210	30	131	18.7	0.811	−0.026
1683 – 1688	20-06-79 – 01-12-79	385	55	149	21.2	0.576	0.741
1713 – 1718	15-09-81 – 26-02-82	385	55	140	20.0	0.147	0.440
1729 – 1734	26-11-82 – 08-05-83	245	35	70.0	10.0	0.361	−0.210
1743 – 1748	12-12-83 – 24-05-84	280	40	61.2	8.75	0.603	−0.386
1760 – 1765	20-03-85 – 31-08-85	245	35	25.0	5.0	0.800	−0.512

black squares at the bottom of the figure show positions of the corresponding time intervals on the curve of smoothed Wolf numbers for cycle 21.

In Figure 1, one can trace how the agreement between the magnetic field and CGLB maps in different latitudinal zones changes over the cycle. The first pair of the maps (upper left-hand side) refers to the ascending branch of cycle 21. One can see a good agreement of the maps in the sunspot formation zone $0-30^\circ$. At the latitudes above 30°, the correlation between the magnetic field and green-line brightness is absent. The next pair of maps in the upper row corresponds to the time interval close to the cycle maximum. Here, the correlation between the maps decreases in the zone $0-30^\circ$ and increases significantly at higher latitudes. The similarity of the next pair of maps decreases at all latitudes. Three lower pairs refer to the descending branch of the cycle. In the zone $0-30^\circ$, the correlation between the corresponding maps increases as the activity minimum is approached. At higher latitudes, one can see a gradual increase of the negative correlation coefficient; i.e., the increase of the magnetic field with latitude is accompanied by a decrease of the green-line brightness.

The correlation coefficients for two latitudinal zones corresponding to the pairs of the synoptic maps in Figure 1 are given in Table I (the last two columns). The table also provides numbers of the Carrington rotations for which the data averaging was performed, the corresponding time intervals, the magnetic field strength in μT, and CGLB in a.c.u. for the maximum-value isolines on the maps, and the steps ΔB and ΔI between the isolines.

3. Magnetic Field Strength and Coronal Green-Line Brightness

Let us consider the cyclic variation of the correlation coefficient r_B between the strength of the magnetic field and the brightness of the coronal green line (see also Badalyan and Obridko, 2004a).

Figure 2 illustrates the time variation of the correlation coefficient in the sunspot formation (upper panel) and high-latitude (lower panel) zones. The thick curves on

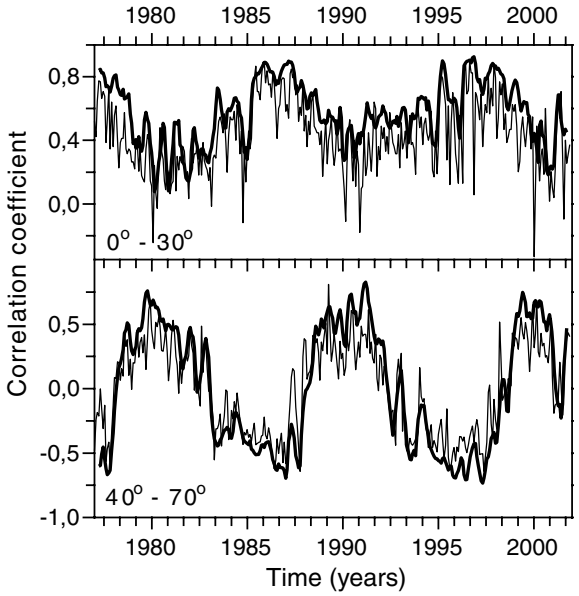

Figure 2. Correlation coefficient r_B in the sunspot formation zone $\pm 30^\circ$ (*top*) and above 40° (*bottom*). The *thin line* shows the correlation coefficients for each particular Carrington rotation and the *thick line* shows the correlation coefficients for the maps averaged over six successive rotations.

both panels show this coefficient for the maps averaged over six successive rotations (represented in Figure 1) at one-rotation steps. One can readily see a cyclic variation of the correlation coefficients r_B calculated separately for the sunspot formation zone $\pm 30^\circ$ and for higher latitudes. Figure 2 shows that r_B variations in these zones occur in anti-phase. In the low-latitude zone, the correlation coefficient is always positive. It reaches high values at the activity minimum and decreases significantly at the maximum. At the mid and high latitudes, on the contrary, r_B reaches large positive values at the maximum and approximately as large but negative values, at the minimum of the cycle. Transition through zero for r_B in the high-latitude zone takes place at the beginning of the ascending branch and at the end of the descending branch of the cycle.

The correlation coefficients for the maps plotted separately for each Carrington rotation (i.e., without averaging over six rotations) are shown with thin lines in both panels of Figure 2. A comparison of two pairs of the curves on each panel shows that the correlation coefficient calculated for the unsmoothed maps is always lesser in absolute value than the coefficient for smoothed maps; it has a greater spread and its variation curve is jagged stronger than in the case of the smoothed maps.

Figure 3 represents the correlation r_B between the magnetic field strength and green-line brightness as a function of the cycle phase Φ. The latter was calculated in accordance with Mitchell (1929) as

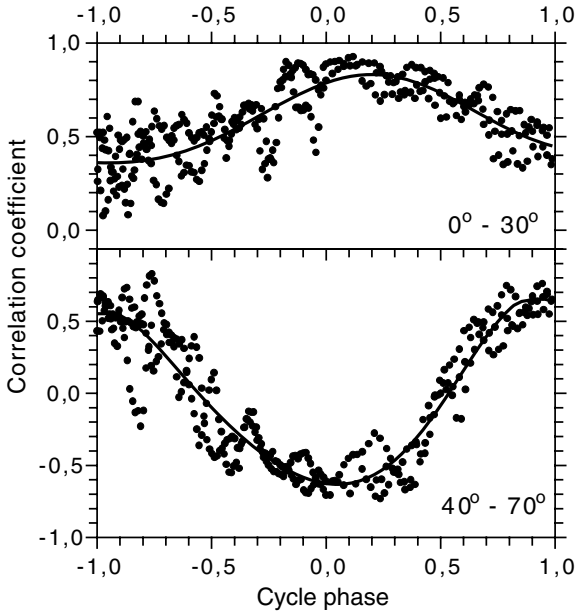

Figure 3. Variation of the correlation coefficient r_B during an activity cycle in two latitudinal zones. It is seen that cyclic variation of r_B is superimposed on short-period oscillations.

$$\Phi = (\tau - m)/(|M - m|). \tag{1}$$

Here, τ is the current time and M and m are, respectively, the nearest maximum and minimum of the 11-year cycle. Thus, according to Equation (1), the phase is 0 at the minimum of each activity cycle, -1 at the maximum of the preceding cycle, $+1$ at the maximum of the following cycle. The phase is positive at the ascending branch and negative at the descending branch of the cycle. Figure 3 illustrates the general variation of the correlation coefficient r_B over a cycle for the sunspot formation zone $\pm 30^\circ$ (upper panel) and the zone above $\pm 40^\circ$ (lower panel). One can see that the mean coefficient varies from about 0.35 at the maximum to 0.85 at the minimum of the cycle in the sunspot formation zone and from $+0.6$ to -0.6, respectively, in the high-latitude zone.

Figures 2 and 3 reveal a pronounced quasi-periodic high-frequency component superimposed on the general time variation of r_B. With the goal of more reliable identification of quasi-periodic variations of the correlation coefficient, we have performed a Fourier analysis, which corroborated the existence of high-frequency (1 – 1.5 years) oscillations of r_B at all latitudes, as well as a noticeable five year wave and 11-year variations.

Figure 4 represents a Fourier periodogram in the latitude–period coordinates for the correlation coefficient r_B in the range of periods from 0.5 to 3 years (upper panel) and to 11 years (lower panel). The upper panel clearly displays oscillations

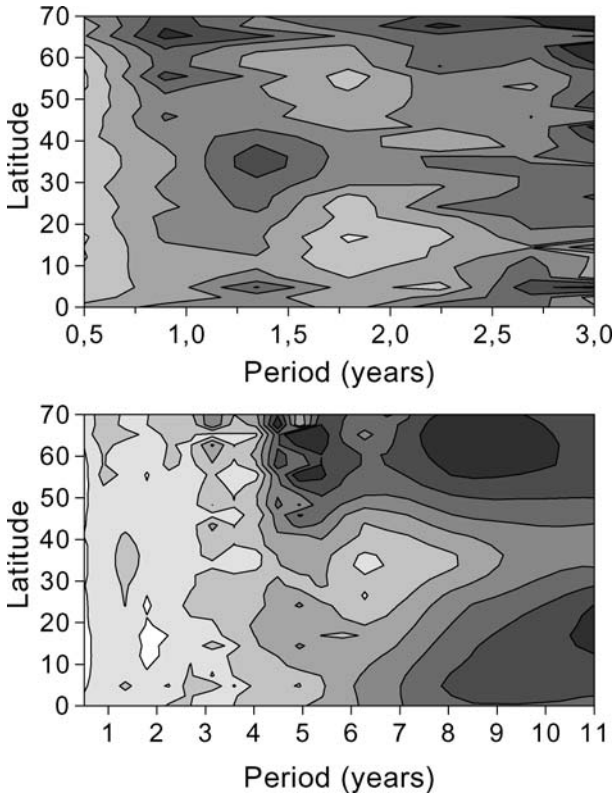

Figure 4. Latitude–period Fourier diagram for the r_B correlation coefficient in the range of periods from 0.5 to 3 years (*top*) and up to 11 years (*bottom*). *Darker regions* correspond to greater oscillation amplitudes.

in the range of 1 – 1.5 years. The oscillation periods of about one year dominate the high latitudes and the periods of about 1.3 years, the low and, particularly, the mid latitudes. It is interesting to note that the period of 1.3 years was revealed by helioseismic methods in the magnetic field generation region in the tachocline (Howe *et al.*, 2000). Here also, the oscillations with a period of 1.3 years are well pronounced at the mid and low latitudes, while at the high latitudes, they seem to be weakened or have smaller period. As for the widely known quasi-biennial oscillations, they are hardly noticeable in the upper panel in Figure 4. It is necessary to emphasize that we analyze the correlation between the magnetic field strength and the coronal green-line emission. Naturally, not all oscillations noticeable in the activity indices will manifest themselves in their correlations.

Unlike the periods of 1 – 1.5 years, r_B oscillations with the periods close to five years are gradually enhanced toward high latitudes. This is seen in Figure 4 (lower panel), which illustrates the low-frequency region. The five year oscillations form a pronounced isolated bulge in the mid-latitude zone. At higher latitudes, the

oscillation amplitude in the low-frequency range, after a certain decrease, begins to grow gradually until it reaches the 11-year period. At lower latitudes, the five year oscillations are weakly pronounced displaying just a gradual increase of the oscillation amplitude in the low-frequency range. The low-frequency part of the Fourier spectrum of the correlation coefficient is weakened significantly in the band of latitudes from 30 to 40°.

The cycle dependence of the correlation coefficient r_B is indicative of different effect of the fields of various scales on the corona brightness. We have revealed not only the cyclic variation of r_B but also the change of sign at high latitudes. This suggests different formation mechanisms of the solar corona in the fields of small, medium, and large scales.

4. Correlation Between the Coronal Green-line Brightness and Magnetic Field Components

Let us discuss the relationship between the green-line brightness and the magnetic field components. Figure 5 represents the time variation of the correlation coefficients for CGLB and the strength of magnetic field and its tangential and radial components (r_B, r_{Bt}, and r_{Br}, respectively). All three correlation coefficients display a pronounced cyclic variation. All coefficients vary in anti-phase in the

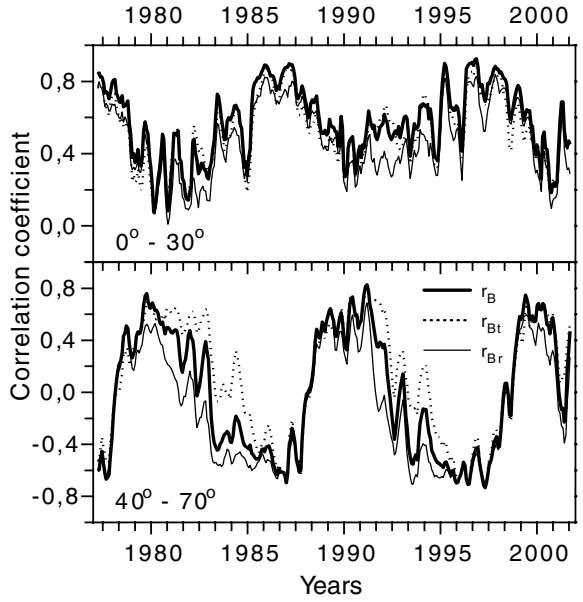

Figure 5. Correlation of the green-line brightness with the strength of the magnetic field r_B and its components r_{Bt} and r_{Br} for two latitudinal zones.

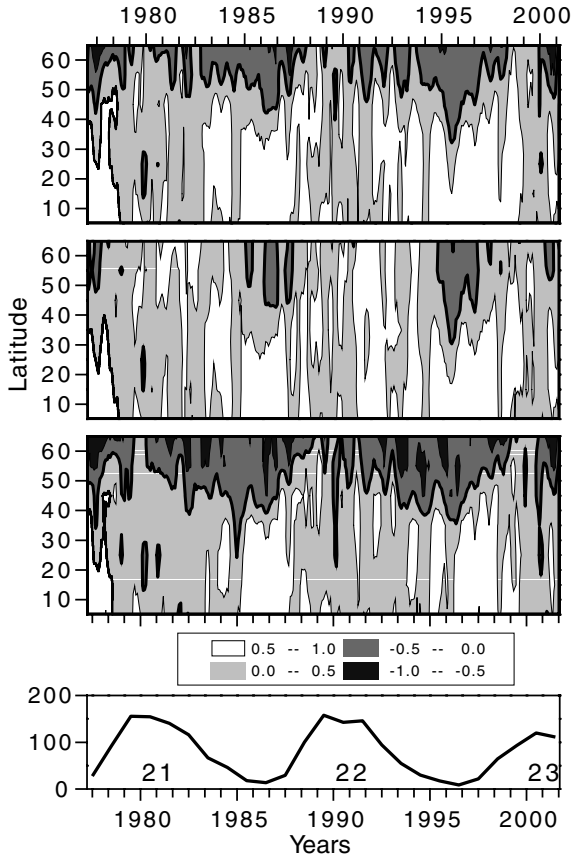

Figure 6. Space–time distribution maps for the correlation coefficients r_B, r_{Bt}, and r_{Br} (from *top to bottom*). The annual mean Wolf numbers and numbers of the activity cycles are given at the *bottom*.

equatorial and high-latitude zones. In the equatorial zone, r_B, r_{Bt}, and r_{Br} are always positive, having the largest values at the minimum of the cycle and decreasing at the maximum. At higher latitudes, the coefficients change their sign, reaching the largest positive values at the maximum of the cycle and the largest negative values, at the minimum.

A closer inspection of Figure 5 reveals some peculiar features in the behavior of the coefficients. One can see that, in the equatorial zone, the correlation of CGLB in the ascending branch is higher with the tangential field component $B_{\rm t}$ than with the radial one $B_{\rm r}$, while in the descending branch, the three coefficients are approximately equal. In the high-latitude zone, the correlation with $B_{\rm r}$ is mainly negative and with $B_{\rm t}$, mainly positive. In the descending branch, the correlation coefficient r_{Br} in this zone exceeds r_{Bt} in absolute value noticeably.

Figure 6 shows the space–time distribution of the correlation coefficients r_B, r_{Bt}, and r_{Br} (from top to bottom) over the latitude band of $\pm 70^\circ$. The

lower panel provides the annual mean Wolf numbers; the figures denote the corresponding activity cycles. The particularities of the time and latitude variations of the coefficients are clearly seen in the diagrams. The thick black line on the maps ("zero correlation line") separates the positive and negative correlation.

One can note that, in the periods of decreasing solar activity, the regions of relatively high positive values of r_B ($r_B > 0.5$, upper map, white color) cover quite a broad latitude band, where they alternate with small areas of the decreased coefficient values. Similar "waves" characterize the increase of the negative values of r_B in the polar zone close to the solar minimum. It is interesting to note the existence of a latitude zone $30-40^\circ$, where the r_B value is close to 0.5 and its cyclic variation is absent. This implies that the boundary between the zones of different time variation of the correlation coefficient lies at the latitude of $\approx 35^\circ$, which is close to the belt of quiet filaments at the cycle minimum. This may be somehow related to the above-mentioned fact that the low-frequency part of the Fourier spectrum of the correlation coefficient is weakened significantly in the latitude zone of $30-40^\circ$.

The typical features in the behavior of r_{Bt} and r_{Br} can also be traced on the maps. It is seen that the regions of $r_{Bt} > 0.5$ in the low-latitude zone are much greater than the similar regions for r_{Br}. On the other hand, the comparison of two lower maps shows clearly that, in the polar zone, r_{Bt} is never larger than 0.5 in absolute value, while the absolute value of r_{Br} exceeds both r_{Bt} and r_B.

Figure 7 represents the cycle dependence of the correlation coefficients r_{Bt} (solid circles and thick curves) and r_{Br} (open circles and thin curves). The figure clearly reveals the cyclic variation of both coefficients. One can also see a small (but systematically repeated from cycle to cycle) difference between r_{Bt} and r_{Br} at the descending branch of activity (negative phase value) in the equatorial zone. In the polar zone, this difference is quite significant, approaching unity. It is interesting to note that, in some places, the short-period variations superimposed on the cyclic variation of both coefficients coincide in different cycles (e.g., on the upper and lower panels of Figure 7 in the phase range from -0.5 to 0). This is indicative of the phase stability of the short-period oscillations in the general scenario of a solar cycle.

Figure 8 shows the latitude–time diagrams of the pair-to-pair differences of the correlation coefficients. A very interesting and significant fact is that the interrelations of the three correlation coefficients (i.e., their differences) form a kind of a stable typical pattern repeated in successive activity cycles. The scales in the right-hand part of the maps show that the coefficient differences differ significantly in magnitude. The difference $r_{Bt} - r_B$ is the greatest, sometimes even exceeding unity. One can see that the correlation of CGLB with B and B_t is very similar everywhere, except for the polar zones, where r_{Bt} becomes smaller in absolute value than r_B (in Figure 8, their difference is negative on the upper panel) at the end of the descending branch. The correlation coefficient for CGLB and B_r at lower latitudes

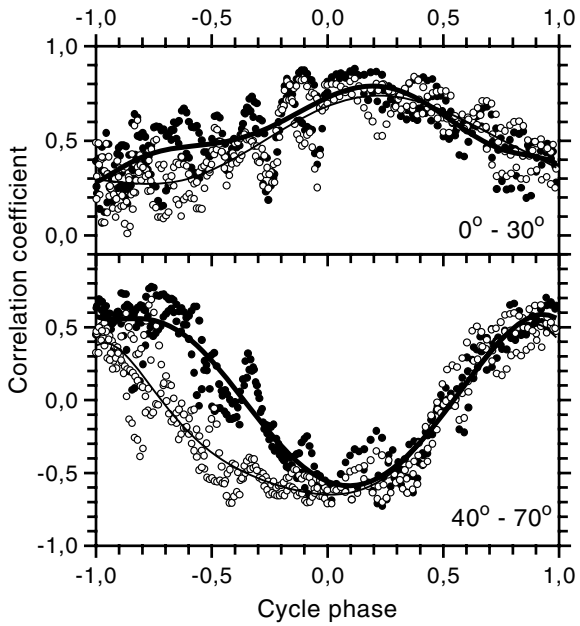

Figure 7. Coefficients r_{Bt} (*solid circles* and *thick curves*) and r_{Br} (*open circles* and *thin curves*) in different phases of the activity cycle.

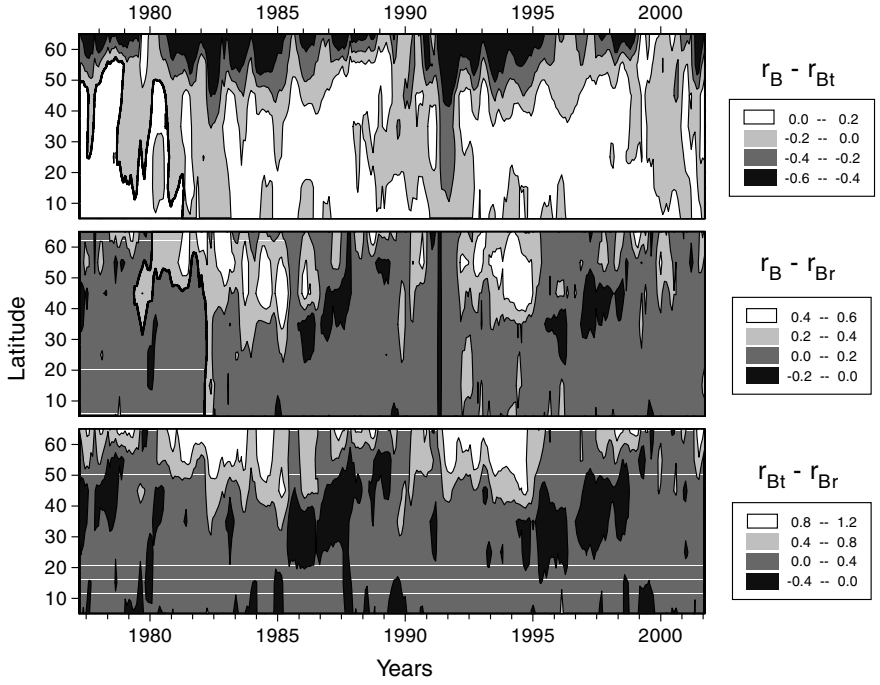

Figure 8. Latitude–time diagrams of the pair-to-pair differences of the correlation coefficients.

is smaller than that for B and B_t (i.e., the differences $r_B - r_{Br}$ and $r_{Bt} - r_{Br}$ are positive). At higher latitudes, r_{Br} at the descending branch and the cycle minimum becomes negative and much greater in absolute value than r_B and r_{Bt}; therefore, their difference in this zone is large positive.

The recurrent distribution pattern of the difference between the correlation coefficients considered above is an evidence of non-casual nature of their temporal and spatial behavior. In other words, this recurrence is indicative of a regular cyclic variation of the latitude–time relationship between CGLB and the magnetic field in the solar corona.

The analysis performed in this section leads us to the conclusion that the main effect on formation of the green-line emission in the latitude zone of $\pm 30^\circ$ is exerted by B_t, which may be due to the presence of low-arch systems filled with dense plasma at the temperature of emission of this line. In the high-latitude zone, particularly at the activity minimum, the effect of B_r is more significant, which is, probably, associated with stronger manifestation of large-scale open magnetic fields.

5. Two-Dimensional Correlation Between the Green-Line Brightness and Magnetic-Field Components

As shown above, the CGLB depends differently on the magnetic field components. Let us consider the coefficient of two-dimensional correlation of B_r and B_t with the green-line brightness. Hereinafter, the coefficient of n-dimensional correlation is the degree of similarity between the initial data set and that calculated by a certain linear model law that describes best the effect of each one of the n independent parameters on the calculated set. The linear law coefficients are found by the n-dimensional least square method.

The dependence between CGLB and magnetic-field components can be represented in the form

$$I_{obs} = c_1 B_t + c_2 B_r + c_3. \tag{2}$$

The parameters c_1, c_2, and c_3 in Equation (2) are calculated by the least square method from the series of data on the green-line brightness I_{obs} and magnetic-field components B_t and B_r for each time interval over six Carrington rotations. Then, knowing the parameters c_1, c_2, and c_3 and the field components B_t and B_r, we can calculate the value I_{cal} at each point of the given latitude–time interval. The correlation coefficient between the calculated I_{cal} and original I_{obs} values of the green-line brightness is called the two-dimensional correlation coefficient. It characterizes the relationship of the line brightness with two field components, while the parameters c_1 and c_2 characterize the contribution of each component in Equation (2).

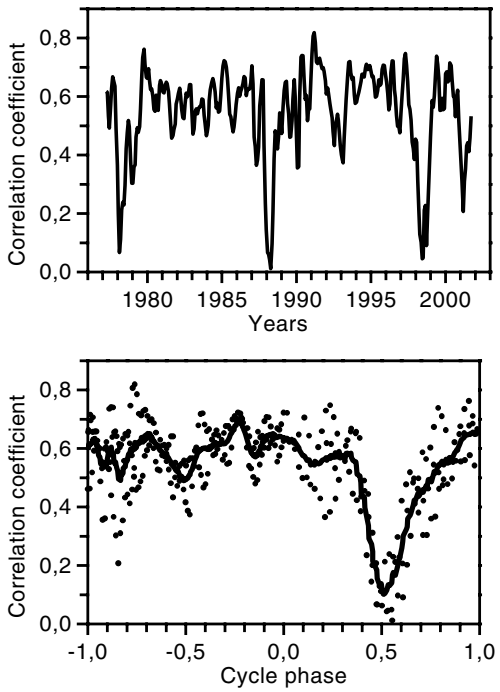

Figure 9. Two-dimensional correlation coefficient (Equation (2)) as a function of time (*top*) and cycle phase (*bottom*) for the high-latitude zone.

The behavior of the two-dimensional correlation coefficient proved to differ in the two latitude zones under discussion. In the sunspot formation zone, this coefficient, in fact, does not differ from the correlation coefficient for CGLB and B.

The behavior of the two-dimensional correlation coefficient in the high-latitude zone $40-70^{\circ}$ is of particular interest. The upper panel in Figure 9 represents the time dependence of the two-dimensional correlation coefficient for the zone in question. As seen from the plot, this coefficient is nearly constant and equals 0.6 (note that the coefficients c_1 and c_2 change over an activity cycle). However, unexpectedly, the figure has revealed some instants of a sharp decrease of the two-dimensional correlation coefficient. On the lower panel of Figure 9, the two-dimensional correlation coefficient is plotted as a function of the cycle phase (Equation (1)). Here, one can readily see that sharp decreases of the coefficient under discussion are quite regular. They occur approximately at the middle of the ascending branch of the activity cycle when the phase is close to $+0.5$. Besides, one can note a slight decrease of the coefficient at the middle of the descending branch, which also is repeated from cycle to cycle.

Thus, it can be asserted that there is a specific time interval during an activity cycle, when the green-line brightness in the high-latitude zone, virtually, does not

depend on the coronal magnetic field. It is interesting to note that this is just the time when the rotation of the solar corona changes: a slow mode appears at high latitudes, and the rotation of the corona becomes pronouncedly differential (Badalyan, Obridko, and Sýkora, 2006).

6. Two Regularities in the Relationship of the Green-Line Brightness with the Magnetic Field and Its Components

As shown above, the character of the relationship between the coronal green-line brightness and magnetic field differs at the low and high latitudes and displays a cyclic variation.

Figure 10 illustrates the time dependence of the green-line brightness and magnetic-field strength in two latitudinal zones. On the lower panel, this dependence is given for the sunspot formation zone $\pm 30^\circ$. Here, both parameters behave in a similar way, increasing toward the maximum and decreasing toward the minimum of activity.

Quite a different picture is seen on the upper panel. In the polar zone $60-70^\circ$, the green-line brightness and magnetic-field strength vary in anti-phase. The former increases at the maximum and decreases at the minimum of the cycle, like at other latitudes. The latter displays an opposite behavior decreasing toward the cycle maximum and increasing toward the minimum.

It is well known that high latitudes are dominated by the large-scale magnetic field, which varies over the cycle just as described above. The fact that the green-line brightness changes in anti-phase with the large-scale field may be explained as follows. It is the large-scale magnetic field that controls the formation of the green-line emission conditions at high latitudes, i.e., the formation of features emitting in the green line. A strong large-scale field produces rarefied features, such as coronal holes. The green-line emission in such features is weakened because of decreased temperature and density. The increasing strength of the large-scale polar field results in the appearance of a greater number of features with the open magnetic configuration.

The coupling of the green-line brightness with the strength of the magnetic field and its components can be represented as a functional dependence. In the vicinity of the activity minimum when the magnetic field has a relatively simple organization, this coupling for the two latitude zones under discussion can be represented as s power-law function of the type

$$I \propto B^q. \tag{3}$$

Examples of such relationship are illustrated in Figure 11. For the sunspot formation zone, the regression line plotted in the upper left-hand part of Figure 11 is described by the formula $I = 0.314B^{0.896}$ (the magnetic-field strength is given in μT and the green-line brightness, in absolute coronal units, a.c.u.). The whole set of the points

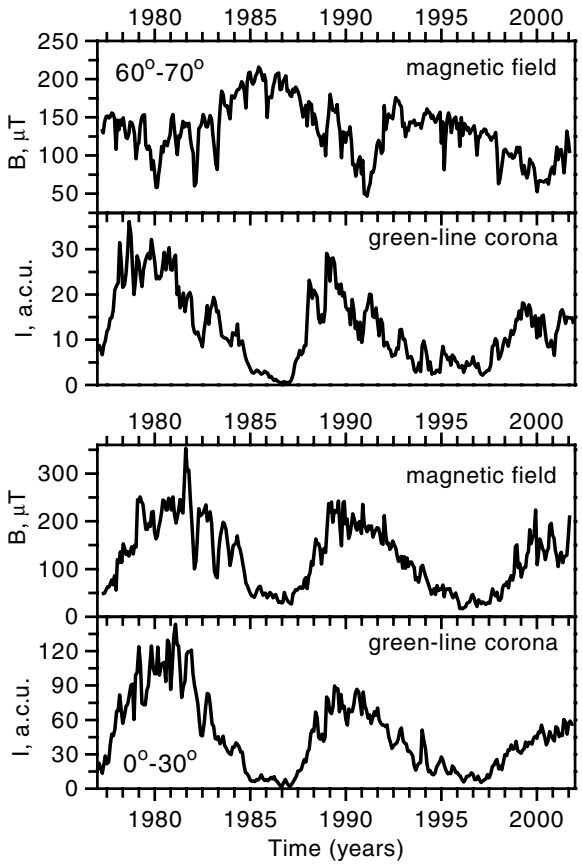

Figure 10. Time dependence of the green-line brightness and magnetic field strength for the equatorial and polar latitude zones.

in this figure refers to the corresponding synoptic map based on the data averaged over rotations 1783 – 1788. It is the early 1987, i.e., the beginning of the activity increase in cycle 22. For the other maps, the power index q is also positive a short time before and immediately after the minimum epochs and changes from 0.75 to 1.00.

In the epoch of solar minimum, the power index q in the zone $40-70^{\circ}$, is negative. On the lower left-hand panel in Figure 11, this dependence is plotted for the map for rotations 1777 – 1782 corresponding to 1986, the minimum of cycle 21. This dependence is well approximated by the formula $I = 71B^{-0.644}$. One can see that the magnetic field strength here is about twice as large as in the low-latitude zone (left-hand upper panel), while the green-line brightness is very low. Therefore, the left-hand lower panel represents the mean values for each north and south latitude at 5° steps, each value being averaged over six Carrington rotations for the given latitude. In spite of a natural ambiguity of each particular CGLB record

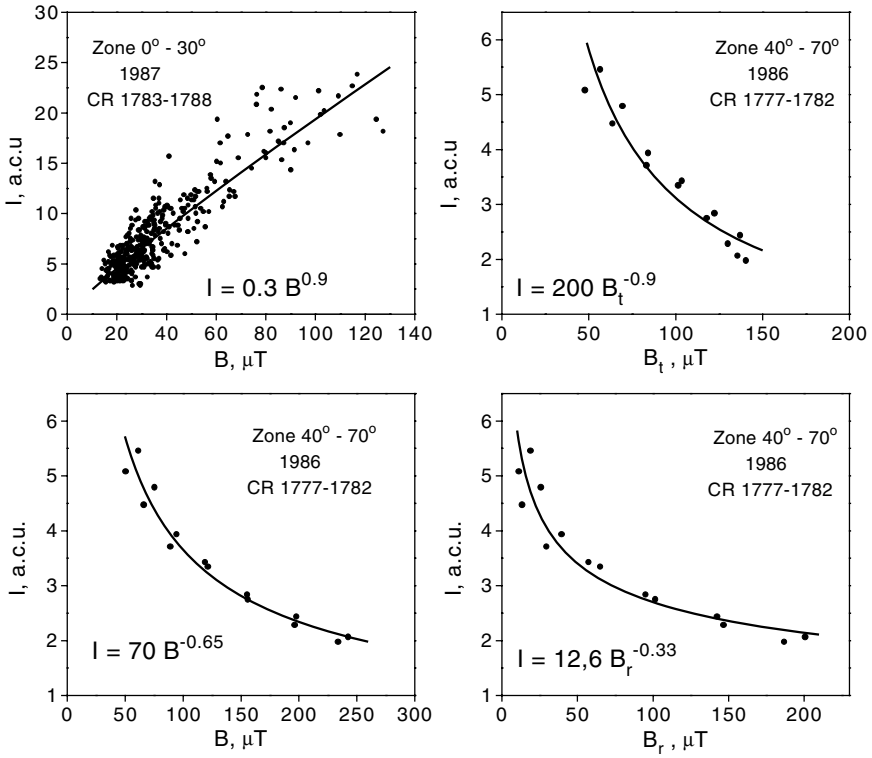

Figure 11. Relationship of the green-line brightness with the strength of the magnetic field and its components.

at high latitudes under weak activity conditions and the accordingly weak emission in the coronal line under discussion, the approximate power-law dependence with a negative index is well defined. On the other maps for the minimum epoch, the power index q ranges from -0.6 to -0.8.

Two right-hand plots in Figure 11 show the relation of the green-line brightness with the tangential (upper panel) and radial (lower panel) field components for the same time interval in the minimum activity epoch, rotations 1777 – 1782. Here (the same as on the plot in the left-hand lower corner), one can see that this relation is described by the power-law function with a negative index. On the other maps, the index q ranges from -0.3 to -0.45 for $B_{\rm r}$ and from -0.75 to -1.05 for $B_{\rm t}$.

Hence, in the vicinity of the activity minimum, the green-line brightness increases nearly linearly with the increase of the magnetic field strength in the equatorial zone and decreases at higher latitudes. This conclusion allows us to put forward some ideas concerning the simulation of the heat balance in the corona.

The heat balance of the corona depends on the energy input-to-loss ratio. In closed magnetic features prevailing in the sunspot formation zone, the energy

balance is determined by heating, radiative loss, and heat conduction. The role of the heat conduction usually is reduced to re-distribution of the thermal energy inside the loop. Therefore, the final loss is mainly determined by radiation (Aschwanden, 2004). Assuming the green-line coronal emission to be proportional to the total radiation flux from the corona, we can directly compare our results with the heating models. Though the heating models involve a great number of the parameters, all of them are interrelated and can be reduced to a single independent parameter – in our case, the magnetic field strength B.

The situation is more complicated at high latitudes, where coronal holes, i.e., features with open magnetic configuration, prevail in the minimum epoch. In this zone, the loss through solar wind exceeds the radiative losses. Therefore, the increase of the solar wind velocity and the area of coronal holes, which grow with the effective increase of the large-scale magnetic field, can result in a decrease of the radiative loss and, accordingly, the coronal emission. However, as seen below, there exist heating models that account for the direct decrease of the coronal brightness with the increase of the magnetic field.

The scaling law in the form of Equation (3) can be applied to the discussion of the coronal heating problem. Mandrini, Démoulin, and Klimchuk (2000) provide the scaling laws, which relate the effective coronal heating H to the magnetic field, loop length and radius, plasma density in the loop, and transverse velocity at the base of the corona. These relations are given for 22 different models. The model of Schrijver *et al.* (2004) was also included in our consideration. Since the relationship between the heating H and the loop length L is known from observations (e.g., Warren and Winebarger, 2006, made a direct comparison of the coronal X-ray emission over the active regions with the magnetic field values and loop lengths), and relationships between other parameters are inferred from theory, the dependencies for all models under discussion can be reduced to a single H–B relation. That is, assuming the coronal emission to be proportional to heating, we can calculate the value q for different models and compare it with observations. It was done in our work (Badalyan and Obridko, 2006) both for the models based on slow field dissipation (DC) and for the wave models based on dissipation of Alfvén waves (AC). All DC models proved to yield very high values of q. For most AC models (Hollweg, 1985; Galsgaard and Nordlund, 1996; Inverarity and Priest, 1995), q is positive. One of the models considered in Ofman, Davila, and Steinolfson (1995) and Ruderman *et al.* (1997) and two wave models described in Halberstadt and Goedbloed (1995) yield negative q values, i.e., these wave models suggest a possibility of negative correlation between the coronal brightness and magnetic field.

It turns out that all mechanisms proposed to explain the observed q values at all latitudes suffer from certain shortcomings. Presumably, a single mechanism of the coronal heating does not exist at all. In each zone on the Sun, the DC and AC mechanisms interact and may yield q with opposite signs. The contribution of each mechanism depends on the structure, spatial dimensions, and strength of

the magnetic field and changes with latitude and phase of the cycle. Our results suggest that at the minimum of the cycle, when the field structure is simple, the wave AC mechanisms dominate at the high latitudes and the DC mechanisms – in the equatorial zone.

7. Conclusions

The coupling between the green-line brightness and the coronal magnetic field and its components has been studied in detail. The mutual correspondence of the synoptic maps for the parameters under discussion has been expressed numerically by the respective correlation coefficients r_B, r_{Bt}, and r_{Br}. The principal results and conclusions are listed below.

1. The analysis of the correlation coefficients in different phases of the cycle and different latitude zones for the period from 1977 to 2001 has shown that the relationship between the coronal brightness and magnetic field strength is not simple and not always unambiguous and that it may, occasionally, change its sign. The correlation between pairs of the synoptic maps for the sunspot formation zone $\pm 30^\circ$ and the latitude zone $40-70^\circ$ displays a cyclic behavior with the corresponding correlation coefficients changing in anti-phase. In the low-latitude zone, the coefficients are always positive. They reach high values at the activity minimum and decrease significantly at the maximum. All three correlation coefficients behave similarly with some minor differences.
2. In the zone above $\pm 40^\circ$, the correlation coefficients reach the largest positive values at the maximum of the cycle. Then, they decrease rapidly passing through zero at the beginning of minimum and become negative at the minimum of the cycle. It should be noted that, in the high-latitude zone, the correlation of CGLB with B_r is noticeably higher in absolute value than the correlation with B and, particularly, with B_t.
3. A two-dimensional correlation coefficient has been calculated for the green-line brightness I and the magnetic field components B_t and B_r. It turned out that, in the high-latitude zone, this coefficient did not, actually, change over a cycle, remaining close to 0.6. On the other hand, we have revealed a particular period in the cycle ascending branch, when the two-dimensional correlation coefficient decreased abruptly. This means that the green-line brightness becomes independent of the magnetic field. In principle, one of the models based on resonance absorption of Alfvén waves (Ofman, Davila, and Steinolfson, 1995; Ruderman *et al.*, 1997) allows such situation.
4. It is shown that, at the activity minimum (when the magnetic field organization is relatively simple), the relation between the green-line brightness

and the strength of the magnetic field and its components can be represented as a power-law function of the type $I \propto B^q$. In the equatorial zone, the power index, and the green-line brightness increases with the increase of the magnetic field strength. At high latitudes, the green-line brightness decreases with the increase of the magnetic field and its components. Here, the power index is negative and does not exceed unity in absolute value.

5. The magnetic field is the basic parameter that controls the formation of various coronal features and creates physical conditions for the green-line emission. These are a sufficiently high density and a temperature of about 2 MK at which the Fe XIV ion exists. The thermal regime of the corona is a result of complex interactions of the mechanisms responsible for the inflow and outflow of matter and energy. As shown by our study, these mechanisms and their interaction differ in different latitudinal zones in the Sun. Accordingly, the conditions of the energy and matter balance in the equatorial and polar zones settled as a result of these interactions are also different. It can be suggested that the energy balance in the equatorial zones is mainly determined by the tangential component of the local fields. The tangential component is believed to hamper (slow down) the outflow of energy and matter and, probably, increase their inflow. A great number of dense, low, high-temperature loops arise due to the tangential component in the low-latitude zone. Here, the green line is bright, and its brightness has a positive correlation with the tangential component. In the high-latitude zone, where the open magnetic configurations (radial component) dominate, the outflow of matter and energy increases, and the dynamic balance is established at a significantly lower temperature and density than at low latitudes. As the magnetic field intensity increases in the vicinity of the activity minimum, the number of such regions grows, the green-line brightness decreases, and the correlation with the radial component is negative. Note that our calculations are based on the steady-state and potentiality assumptions and, therefore, they do not apply to the nonstationary corona over sunspots.

The results obtained in our work may be used for quantitative testing of various models of the corona heating.

Acknowledgements

We are grateful to M. A. Livshits and J. Sýkora for discussion of some questions touched upon in this paper. The work was supported by the Russian Foundation for Basic Research, Project nos. 05-02-16090 and 05-02-170.

References

Aschwanden, M.J.: 2004, *Physics of the Solar Corona: An Introduction*, Praxis Publishing, Chichester, UK.

Badalyan, O.G. and Obridko, V.N.: 2004a, *Astron. Zh.* **81**, 746 (English translation *Astron. Rep.* **48**, 678).

Badalyan, O.G. and Obridko, V.N.: 2004b, in A.V. Stepanov, E.E. Benevolenskaya, and A.G. Kosovichev (eds.), *Multi-Wavelength Investigations of Solar Activity*, *IAU Symp.* **223**, 371.

Badalyan, O.G. and Obridko, V.N.: 2006, *Astron. Lett.* (in press).

Badalyan, O.G., Obridko, V.N., and Sýkora, J.: 2004, *Astron. Astrophys. Trans.* **23**, 555.

Badalyan, O.G., Obridko, V.N., and Sýkora J.: 2005, *Astron. Zh.* **82**, 535 (English translation *Astron. Rep.* **49**, 477).

Badalyan, O.G., Obridko, V.N., and Sýkora, J.: 2006, *Astron. Zh.* **83**, 352 (English translation *Astron. Rep.* **50**, 312).

Fisher, R. and Musman, S.: 1975, *Astrophys. J.* **195**, 801.

Galsgaard, K. and Nordlund, A.: 1996, *J. Geophys. Res.* **101**, 13445.

Guhathakurta, M., Fisher, R.R., and Altrock, R.C.: 1993, *Astrophys. J.* **414**, L145.

Guhathakurta, M., Fisher, R., and Strong, K.: 1996, *Astrophys. J.* **471**, L69.

Halberstadt, G. and Goedbloed, J.P.: 1995, *Astron. Astrophys.* **301**, 559.

Hoeksema, J.T.: 1991, *Solar Magnetic Fields – 1985 Through 1990*, Report CSSA-ASTRO-91-01, Center for Space Science and Astronomy, Stanford University.

Hoeksema, J.T. and Scherrer, P.H.: 1986, *The Solar Magnetic Field – 1976 Through 1985*, WDCA Report UAG-94, NGDC, Boulder, CO.

Hollweg, J.V.: 1985, in B. Buti (ed.), *Advances in Space Plasma Physics*, World Scientific, Singapore, p. 77.

Howe, R., Christensen-Dalsgaard, J., Hill, F., Komm, R.W., Larsen, R.M., Schou, J., Thompson, M.J., and Toomre, J.: 2000, *Science* **287**, 2456.

Inverarity, G.W. and Priest, E.R.: 1995, *Astron. Astrophys.* **302**, 567.

Kharshiladze, A.P. and Ivanov, K.G. : 1994, *Geomagnet. Aeron.* **34**(4), 22 (in Russian).

Letfus, V., Kulčár, L., and Sýkora, J.: 1980, in M. Dryer and E. Tandberg-Hanssen (eds.), *Solar and Interplanetary Dynamics*, *IAU Symp.* **91**, 49.

Mandrini, C.H., Démoulin, J., and Klimchuk, A.: 2000, *Astrophys. J.* **530**, 999.

Mitchell, S.A.: 1929, in G. Eberhard, A. Kohlschütter, and H. Ludendorff (eds.), *Handbuch der Astrophysik*, Vol. 4, Springer, Berlin, p. 231.

Obridko, V.N. and Shelting, B.D.: 1999, *Solar Phys.* **184**, 187.

Ofman, L., Davila, J.M., and Steinolfson, R.S.: 1995, *Astrophys. J.* **444**, 471.

Ruderman, M.S., Berghmans, D., Goosens, M., and Poedts, S.: 1997, *Astron. Astrophys.* **320**, 305.

Rušin, V. and Rybanský, M.: 2002, *Solar Phys.* **207**, 47.

Schrijver, C.J., Sandman, A.W., Aschwanden, M.J., and DeRosa, M.L.: 2004, in F. Favata, G.A.J. Hussian, and B. Battrick (eds.), *Proceedings of the 13th Cambridge Workshop on Cool Stars, Stellar Systems and the Sun, ESA SP-560*, p. 65.

Storini, M. and Sýkora, J.: 1997, *Nuovo Cimento* **20C**, 923.

Sýkora, J.: 1971, *Bull. Astron. Inst. Czechosl.* **22**, 12.

Sýkora, J.: 1992, *Solar Phys.* **140**, 379.

Sýkora, J. and Rybák, J.: 2005, *Adv. Space Res.* **35**, 393.

Wang, Y.-M., Sheeley, N.R., Jr., Hawley, S.H., Kraemer, J.R., Brueckner, G.E., Howard, R.A., Korendyke, C.M., Michels, D.J., Moulton, N.E., and Socker, D.G.: 1997, *Astrophys. J.* **485**, 419.

Warren, H.P. and Winebarger, A.R.: 2006, *Astrophys. J.* **645**, 711.